Available online at www.sciencedirect.com

ScienceDirect

Ceramics International 41 (2015) 10116–10124

CERAMICS INTERNATIONAL

www.elsevier.com/locate/ceramint

Tuning the morphology of ZnO nanostructure by in doping and the associated variation in electrical and optical properties

M.A. Awad[a,*], A.M. Ahmed[a], V.O. Khavrus[b], E.M.M. Ibrahim[a]

[a]Physics Department, Faculty of Science, Sohag University, Sohag 82524, Egypt
[b]Leibniz Institute for Solid State and Materials Research (IFW), PO Box 270016, Dresden D-01171, Germany

Received 15 March 2015; received in revised form 18 April 2015; accepted 19 April 2015
Available online 25 April 2015

Abstract

In this work, $Zn_{100-x}In_x$ ($x=0$, 1, 2.5, 5 and 7.5 at%) compounds have been initially alloyed by melting method and used as precursors to prepare different nanostructures of indium (In) doped ZnO using chemical vapor deposition (CVD). The effect of In content on the structural, morphological, optical as well as electrical properties has been studied. XRD and Raman examinations demonstrate the substitution of Zn^{+2} ions by In^{+3} ions at lower indium concentrations, while In_2O_3 appears as separate phase at higher In ratios. The nanowires transform to nanoflakes then nanoflowers as the In concentration increases. With regard to the optical properties, the transparency increases with increasing In and decreases thereafter. The optical band gap values increase with In content reaching its maximum value (3.28 eV) for the sample of $x=5$ at%. The refractive index, extinction coefficient and Urbach tail are also affected by In doping. The electrical conductivity enhances at lower doping level due to formation of thermally activated donor levels, despite this, the phase separation and phonon scattering are factors responsible for conductivity decrease at higher In content.

Keywords: C. Electrical conductivity; C. Optical properties; In-doped ZnO; Nanowires; Raman spectra

1. Introduction

Recent interest on the development of nanostructures devices for various applications has generated a huge thrust on the development of semiconductor nanostructures of adequate morphologies and compositions [1]. Nanowires (NWs), in particular, now span a broad range of applications including diodes, field effect transistors, logic circuits, single electron transistors, optoelectronic devices, sensors, thermoelectrically devices, photocatalysis and piezoelectronics. In these realms, NWs structures exhibit unique and superior properties compared to their bulk counterpart's properties, where their 1D confined transport of electrons or photons, large surface area, quantum confinement and excellent mechanical properties play major roles [2].

ZnO is considered as excellent candidate for various applications; it is n-type semiconductor due to the presence of intrinsic defects (oxygen vacancies, zinc vacancies and zinc interstitials [3]. It has a number of advantages that attract the researchers' attention such as good electrical and optical properties [4]. Also it is an attractive material in the field of transparent conductive oxides (TCOs). Despite these features, there are some properties don't meet requirements for some industrial fields [4]. Hence the necessity to dope ZnO with various elements becomes key demand. The hexagonal close-packed lattice of ZnO with empty octahedral sites enables the dopant to be incorporated and tune the electrical, optical and magnetic properties [5]. Indium is recognized as one of the most efficient elements used to enhance the optoelectronic properties of ZnO because it improves the optical transmission and the electrical conductivity [3] as well as decreases the reactivity with oxygen. It was previously considered that In doped ZnO is highly transparent and electrically conductive n-type semiconductor [6]. Also, using In as a dopant is

*Corresponding author. Tel.: +201121391658; fax: +20934601159.
E-mail address: arwamadeha@yahoo.com (M.A. Awad).

http://dx.doi.org/10.1016/j.ceramint.2015.04.108
0272-8842/

unique because it induces some structural defects that form different morphologies [7,8].

According to our knowledge, so far, alloys of Zn–In as source material prepared by melting technique have not been reported yet. Therefore, in this paper alloys of In doped ZnO with different concentrations of indium were prepared by melting technique and were used as source materials. The effect of indium content on morphology, optical, electrical properties as well as crystallinity of the material was studied.

2. Experimental procedure

2.1. Fabrication of the source materials

To fabricate In doped ZnO nanostructures using vapor transport, bulk alloys of In_xZn_{100-x} (x=0, 1, 2.5, 5 and 7.5 at%) were manufactured by melting technique to be used as source materials. For this purpose, granules of In and Zn (99.9999% purity) were weighed according to their atomic percentages and sealed in quartz ampoules under pressure of $\sim 10^{-5}$ mbar to avoid any reaction with oxygen or residual gases. The sealed ampoules were kept inside the furnace where the temperature was adjusted at 600 °C for 12 h with shaking at regular time intervals (1 h) to ensure homogenous mixing of the constituents. After that, the furnace was cooled down to room temperature. Each produced ingot of the bulk product was cut separately to small granules with average diameter (~2 mm).

2.2. Fabrication of In doped ZnO nanostructures

To fabricate ZnO nanostructures with different In content, five sets of undoped and In-doped ZnO were placed separately in alumina boat positioned at the center of the heating zone of horizontal furnace (internal diameter of 36 mm and length of 54 cm). The synthesis was carried out on two different kinds of substrates, specifically Au coated (25–30 nm) Si (1 0 0) and quartz substrates (cut into 1 cm × 1 cm and ultrasonically cleaned). The prepared substrates were located longitudinally inside the horizontal furnace 4 cm away and along 16 cm distance from the source. The gaseous precursors were carried to the substrates using a mixture of high purity (99.99%) Ar and O_2 (20:1) gases with flow rates of 200 and 10 sccm, respectively. The furnace temperature was raised gradually to 900 °C and held for 30 min at this temperature. The substrates temperatures ranged from 660–875 °C during the deposition. Note that the high temperature of the substrates is necessary for enhancing the crystallinity of the deposited material.

XRD type Shimadzu Diffractometer XRD 6000, which utilizing Cu$K\alpha$ radiation (λ=1.54056 Å) and scanning electron microscope SEM (type JOEL model JSM-6380 LA), were utilized to examine the crystal structure and morphology of In doped ZnO nanostructures, respectively. Elemental analysis for the products was performed using energy dispersive analysis of X-ray (EDAX) unit attached with the SEM. Raman spectroscopy was performed using a Thermo Scientific DXR Smart Raman spectrometer with an excitation wavelength of 532 nm and a laser power of 8 mW. The transmission (T) and reflection (R) were measured using Jasco V-570 double beam spectrophotometer for photons wavelengths ranges from (200–2500 nm) at normal incidence. The spectra were recorded at room temperature. The electrical conductivity was measured using the so called four probe method, where the outer probes were used for current passing, and the inner probes were connected to stabilized power supply type FARNELL INSTRUMENTS LTd. The current which was supplied by this power supply was measured by digital multimeter type PROTEK A-445 with sensitivity 0.01 μA.

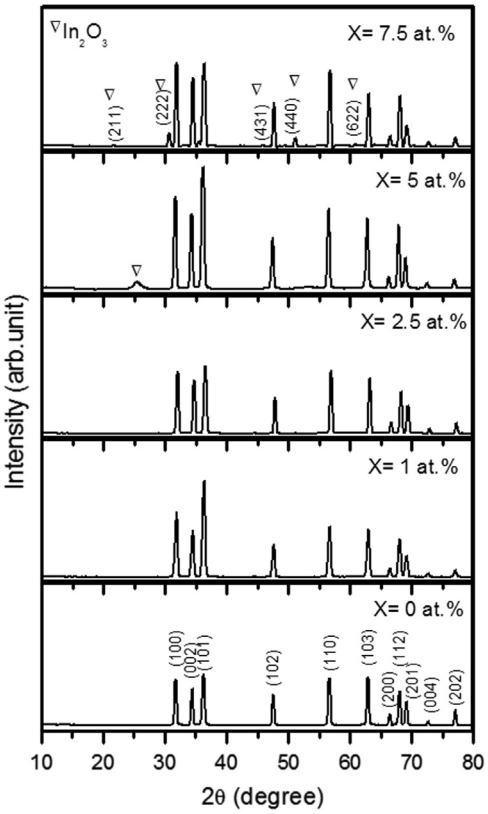

Fig. 1. XRD patterns on Au coated quartz substrates for undoped and In-doped ZnO nanostructures.

3. Results and discussion

3.1. Structural examinations

XRD analysis for undoped and In-doped ZnO nanostructures was performed for assessing the overall structure and phase purity (see Fig. 1). For the undoped sample (x=0.0) all the diffraction peaks are indexed to hexagonal wurtzite structure of ZnO (JCPDS card no. 79-0206) with lattice parameters $a=3.248 \pm 0.005$ Å and $c=5.20 \pm 0.005$ Å. No additional peaks correspond to Zn or other impurities were observed. The sharpness of most peaks confirms the good crystallinity of the product. With 1 at% indium addition, the intensity of most peaks increased to some extent which might be due to indium incorporation in the interstitial sites of ZnO lattice. There are reorientation for most peaks appears with In

content = 2.5 at% and ascribed to the substitution of Zn atoms by In. Similar results were obtained by Morales et al. [1] for indium doping ratios (x = 3 and 5 at%). It is worth mentioning that lower doping of indium (x = 1 and 2.5 at%) doesn't lead to appearance of another phases such as In_2O_3 or In, asserting that In is successfully incorporated into ZnO lattice with no evident of residual stress or inclusion-induced lattice distortion [9].

Further doping of In (5 at%) leads to increase of the intensity of the peaks with appearance of a new peak at $2\theta = 25^\circ$ related to indium oxide (JCDPS card no. 01-0929). Similar results were reported for In–ZnO with the same indium content by Badadhe et al. [10]. From the aforementioned results, one can conclude that, at lower doping, indium atoms distribute uniformly in the ZnO nanostructures making an orderly arrangement with growth enhancement of ZnO along (1 0 1) and (1 0 0) directions [9,11]. For the highest doping level of indium (the alloy of x=7.5 at%), five new peaks are observed (JCDPS card no. 76-0152), and all belong to In_2O_3. The presence of In_2O_3 peaks indicates that the indium addition, instead of being incorporated in the ZnO nanostructure, remained phase separated, at least partially. There are a small shift towards lower 2θ for x=5 at% as compared with those of the undoped ZnO nanostructure with lattice constant (a=3.26 ± 0.005 Å and c=5.22 ± 0.005 Å). The peaks shifts can be attributed to lattice expansion induced by In^{3+} incorporation which has relatively bigger ionic radius (0.81 Å) compared to that of Zn^{2+} ions (0.74 Å) [4].

In wurtzite-type ZnO which belongs to the space group $C6v$, the optical phonons at the Γ point of the Brillouin is characterized by the representation, $A_1 + 2B_1 + E_1 + 2E_2$. In this representation, both A_1 and E_1 modes are polar and split into transverse optical (TO) and longitudinal optical (LO) phonons, with all being Raman and infrared active. The nonpolar $E_{2(High)}$ modes are the Raman active, while the B_1 mode is the silent one. Fig. 2 shows the Raman spectra for the undoped and In doped ZnO ranging from 200 to 800 cm^{-1}. The data confirm that the prepared samples are characterized by the wurtzite-type structure due to appearance of the high frequency $E_{2(High)}$ mode at Raman shift 433 cm^{-1} [12]. It was found that the area of the Raman line $E_{2(High)}$ is more or less unchanged with In doping. The Raman lines appear at 327 and 376 cm^{-1} correspond to the $2E_{2(M)}$ mode and the TO mode with A1 symmetry, respectively. Compared with ZnO, the intensity of these peaks doesn't change in the doped materials. The fixed areas and intensities of the peaks confirm that when the In^{+3} ions substitute Zn^{+2} ions, no deformation occurs in the internal structure of the ZnO due to that the radius of Zn^{+2} and In^{+3} are approximately the same. In Fig. 2, one additional peak clearly appears at Raman shift 580 cm^{-1} on the spectrum of the x = 2.5 at% sample and its intensity increases as the In content increases to 7.5 at%. This peak belongs to the In_2O_3 separate phase [13]. Note that, appearance of the In_2O_3 phase for x = 5 and 7.5 at% samples coincide well with the aforementioned XRD results. However, it was not observed by the XRD investigation for the sample x = 2.5 at% because of the sensitivity limit of the measurement. From the results of XRD and Raman spectra, it can be deduced that, although substitution of In^{+3} for Zn^{+2} ions leads to a change of the samples morphology (as will be demonstrated by SEM investigation in the next section), it doesn't change the wurtzite ZnO structure. Additionally, they confirm the In_2O_3 phase separation at certain In doping level of ZnO nanostructures.

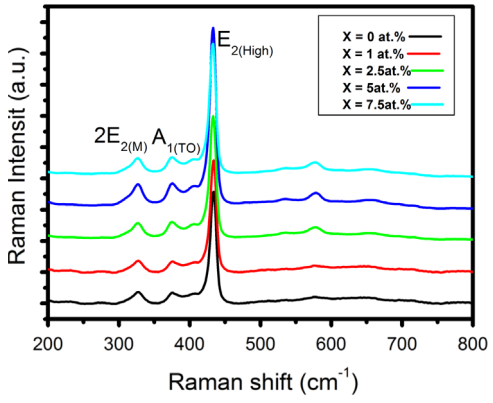

Fig. 2. Raman spectra of undoped and In-doped ZnO nanostructures.

3.2. Morphology and chemical composition examinations

SEM images with low and high magnifications for undoped and In-doped ZnO nanostructures prepared on Si (1 0 0) substrates are shown in Figs. 3a–d and 4a–d, respectively. Clearly, the undoped samples (Fig. 3a and b) are randomly oriented nanowires NWs with diameters range from 100 to 350 nm, and length of several micrometers. There are little amount of nanoparticles formed on the surface of the NWs. The randomization of the nanowires is due to the mismatch between the wire lattice and the substrate which changes the growth direction of the NWs and thus influences the final morphologies [2]. Furthermore, it was observed that indium ions incorporation changes the morphology and redirect the growth of ZnO nanowires, where adding 1 at% of indium (Fig. 3c and d) changes the morphology mainly to stacked nanoflakes. The width of the flakes reaches 500 nm which is higher than the diameters of the undoped nanowires. Noteworthy, increasing the diameter enhances the crystallinity because it leads to reduction in the strain [14] and this is in consistent with the XRD results of our materials. Yousefi et al. [15] obtained nanoflakes shape of In-doped ZnO but with higher concentration of indium (8 at%). The optimum In content for preparing nanoflakes of In–ZnO may differ according to the source material (here we utilized alloy of In doped ZnO). Doping with 2.5 at% of indium (Fig. 4a and b) catalyzes the nanoflakes to group together forming flower-like morphology. The petals of the flower are like needles in shape with average diameter 100 nm at the tip and 2 μm at the base. Similar result obtained by Morales et al. [1] with indium concentration (x = 2 at%) using hydrothermal process. Further doping of In (x = 7.5 at%) enhances the growth of the nanoflowers perpendicular to the substrate (Fig. 4c and d). The growth mechanism of the undoped and In doped ZnO nanostructures may be explained as follows: the plane [0 0 0 1] is called the basal plane, which is the most commonly used surface for growth. According to Lim et al. [4] and Li et al. [16], ZnO has the fastest crystal growth velocity in the [0 0 0 1]

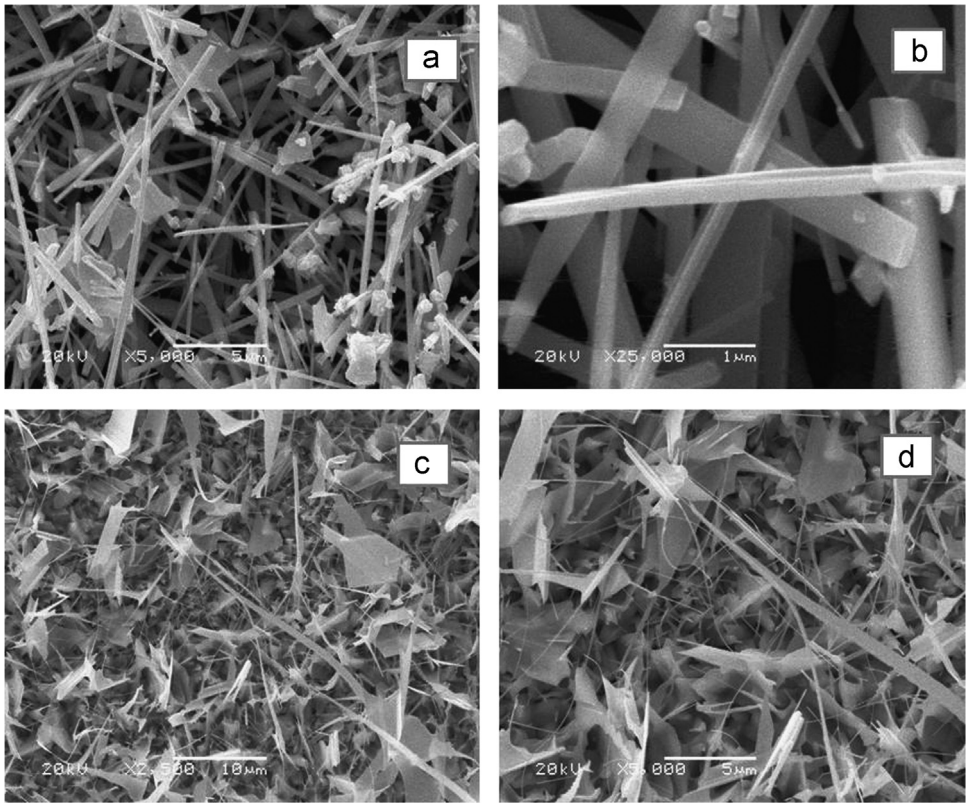

Fig. 3. Low and high magnifications SEM images for undoped (a, b) and 1 at% In doped (c, d).

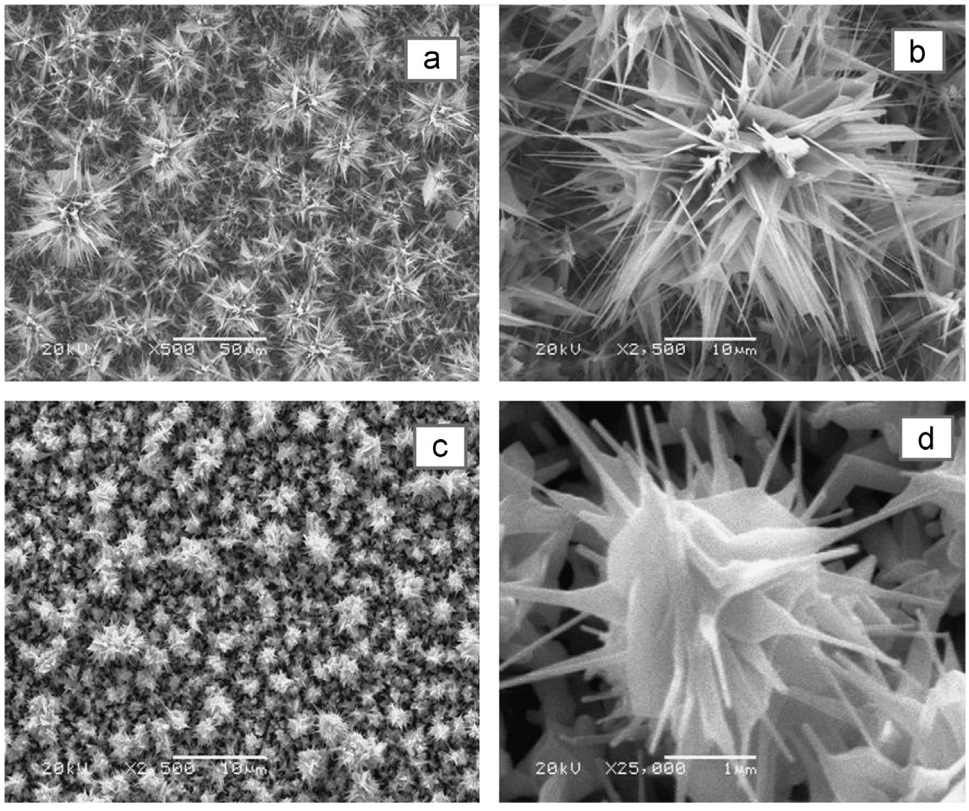

Fig. 4. Low and high magnifications SEM images for 2.5 at% In (a and b) and 5 at% In doping (c and d).

direction due to its high surface energy. The velocity of the crystal growth varies in different directions and is governed by $V_{[0\,0\,0\,1]} > V_{[0\,1\,\bar{1}\,0]} > V_{[0\,0\,0\,\bar{1}]}$. Addition of indium leads to redistribution of the surface energy and growth direction, where the growth along [0 0 0 1] decreases leading to formation of nanoflakes and hence nanoflowers. This means that In acts as passivation agent by charge compensation and slow the growth of ZnO along the [0 0 0 1] direction [4].

The amount of In doping concentration was determined using the EDAX elemental analysis and the data are tabulated in Table 1. Clearly, indium concentration increases at the expense of Zn indicating the replacement of Zn atoms by In atoms in the composition. The presence of low percentages of In compared to which were utilized in the starting In–Zn alloys is attributed to the limited indium solubility in ZnO lattice, and any excess of indium content makes a phase separation as was confirmed by the XRD results stated above. Also the low vapor pressure of indium atoms compared to Zn atoms reduces the chance of indium species existence in the ambient of the reaction.

3.3. Optical properties

Fig. 5a depicts the transmission (T) spectra of ZnO nanostructures with different In content. The data imply that the transparency is high in the visible to near-infrared ranges which is typical feature of semiconductors. The transmission increases as the In content increases. To be specific, the maximum transmission obtained around 70–90% in visible to near infrared region for indium content $x=5$ at%. The decrease in transmittance at higher doping concentrations ($x=7.5$ at%) may be due to increase of photons' scattering by crystal defects created by doping [9] as well as the increase of the charge carriers concentrations.

There is no transmission features could be detected in the UV- region, because of the electrons transfer to the conduction band (electronic absorption), where the lower limit of transmission range coincides closely with the wavelength of the fundamental band gap [17]. There is a shift in the absorption edge towards lower wavelengths from $x=0$ to 5 at% which can be attributed to the increase of the band gap as will be shown later. Note that, the absorption edge of ZnO is much higher (in wavelengths) than that of the glass substrates so the absorption edge shown in Fig. 5 is from the ZnO films, but not from glass substrates. Noteworthy, the transparent region between the infrared and ultraviolet absorption bands is useful for many applications particularly for making optical windows and lenses [17].

The reflection spectra (Fig. 5b) behave approximately in opposite manner of transparency where the reflectivity is high in the wavelength range (400–500 nm). Note that, the lowest reflectivity in visible region is for $x=5$ at%.

Using transmossion, reflection and film thickness values, the absorption coefficient was calculated by the following equation:

$$\alpha = \frac{1}{d}\ln\left(\frac{1-R}{T}\right) \quad (1)$$

Table1
Element concentration, optical band gap and Urbach energy (E_u) for undoped and In doped ZnO.

x (at%)	Element concentration (%)			E_g (eV)	E_u (meV)
	Zn	O	In		
0	52.25	47.75	–	3.18	705
1	51.50	48.35	0.15	3.27	709
2.5	50.44	48.68	0.88	3.28	822
5	50.06	48.53	1.41	3.29	887
7.5	48.31	49.49	2.20	3.28	910

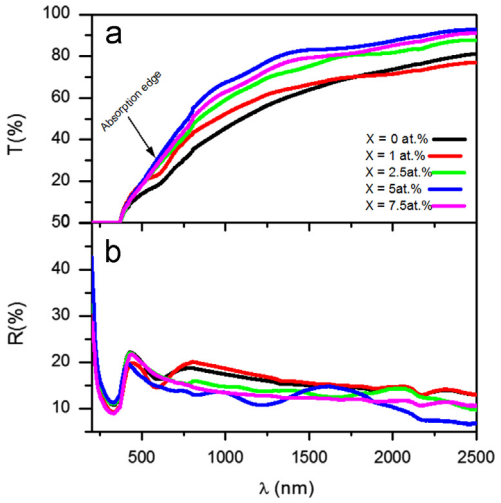

Fig. 5. The transmission (T%) and reflection (R%) curve as a function of wavelength and In content for In-doped ZnO nanostructures.

where R, T and d are the reflectivity, transmission and film thickness, respectively.

The optical band gap was estimated from Tauc relation [18]

$$(\alpha h\nu) = \beta\left(h\nu - E_g\right)^{\eta} \quad (2)$$

where β is constant, and η equals to 2 or 1/2 for indirect and direct transition, respectively. Herein direct allowed transitions are applied. The E_g values were obtained by extrapolating the linear part of $(\alpha h\nu)^2$ versus the photon energy as shown in Fig. 6. The estimated values are plotted in Fig. 7. For indium contents of $x=0$, 1, 2.5 and 5 at%, the optical band gap increases as the In content increases. The observed widening of the optical band gap is generally attributed to Burstein–Moss shift [19] which means that by increasing donors concentration, new states being populated with electrons in the conduction band and thus the optical band gap increases. At doping level of $x=7.5$ at%, the band gap decreases slightly, because the lowest state in the conduction band is blocked which is responsible for the widening in the optical band gap [11]. The new incoming donor species populate the states near the conduction band, subsequently the donor and conduction bands merge and thereby the Fermi level shifts upwards near the conduction band. It was previously considered that the decrease of the band gap may be related to the band tailing,

electron–electron and electron–ion interaction [20]. It is worth mentioning that, values of the optical band gap of our compositions (Table 1) are smaller than that of single crystalline ZnO (band gap of 3.3 eV). It should be taken in consideration that variation of the band gap in films depends on many factors such as existence of growth stress, thermal expansion mismatch stress and dopants [21,22].

The dispersion curves of the In doped ZnO nanostructures are presented in Fig. 8. From 500–2500 nm, the refractive index (n) decreases with increasing the wavelength for most samples showing normal dispersion. In the UV-region, the refractive index changes irregularly with the wavelength

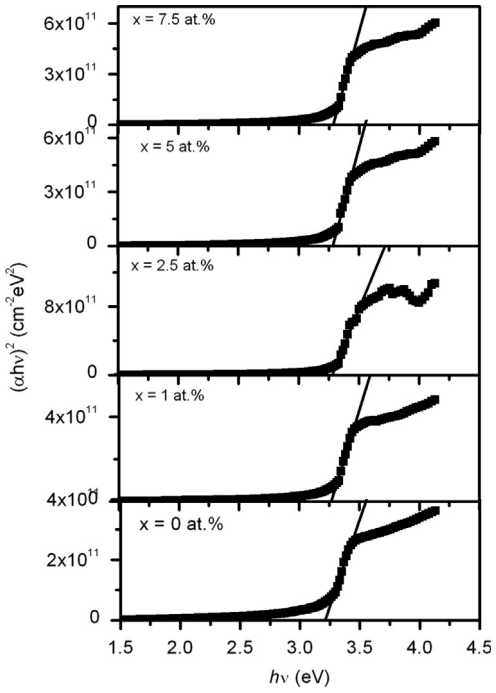

Fig. 6. $(\alpha h\nu)^2$ vs. $h\nu$ plots of the synthesized undoped and In-doped ZnO nanostructures.

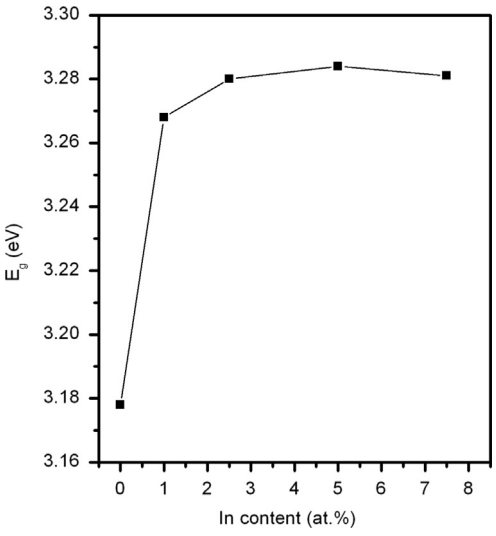

Fig. 7. Variation of the optical band gap E_g with In content for the synthesized materials.

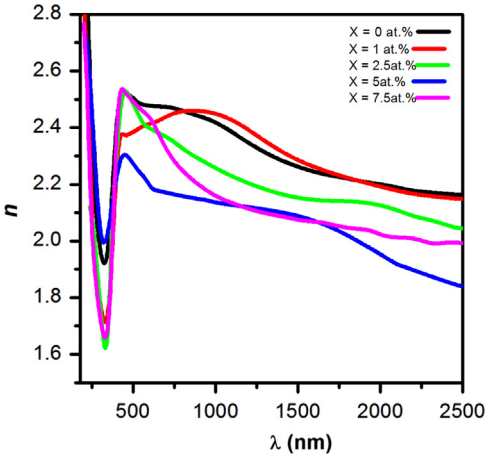

Fig. 8. Refractive index as functions of wavelength for undoped and In-doped ZnO nanostructures.

(anomalous dispersion) due to the high absorption. Over most of the measured wavelength range, the n values decrease with In content according to the increase in transparency. The lowest refractive index was obtained for $x=5$ at% which has the highest transparency.

The extinction coefficient (k) is directly related to the absorption coefficient by the relation

$$k = \frac{\alpha\lambda}{4\pi} \tag{3}$$

where α is the absorption coefficient and λ is the photon wavelength. As known, extinction coefficient depends strongly on both the energy of the incident photon and impurities in the substance, where absorption occurs only if the photon energy equals or higher than the optical band gap. The extinction coefficient decreases with increasing indium content in visible to near IR region, as shown in Fig. 9, due to the band widening. The lower extinction coefficient obtained for In content with $x=5$ at%. Extinction coefficient is high in UV-region because of the electronic absorption. Palmer et al. [22] proposed that in some TCOs, the donor and acceptor pairs in the substance could cause a band gap narrowing which offset the Burstein–Moss effect. This theory is predominant in our compositions in the UV region, where the absorption increases with indium increasing due to the band gap narrowing (increasing dopant). The maximum absorption peak is at approximately 380 nm for all the samples.

The absorption behavior at lower photon energy can be represented by Urbach equation:

$$\alpha = K_{exp}\,(E/E_u) \tag{4}$$

where K is constant, E is photon energy and E_u is Urbach energy which is interpreted as the width of the tails of the localized states in the band gap [23]. The absorption in this region can be ascribed to existence of structure disorder induced by defects and doping [23] leading to transitions between extended states in one band and localized states in the exponential tail of the other band [24]. The E_u values, obtained by plotting $\ln\alpha$ as a function of photon energy (Fig. 10) and listed in Table 1, increase with In content. The relatively large

increase of E_u observed with the increase of In content from $x=2.5$–7.5 at% may be attributed to the increase of point defects induced by In_2O_3 formation [23] which has been confirmed by aforementioned Raman and XRD analyses. The increase in E_u values with increasing In doping has been reported previously by Tokumoto et al. [23] for indium doped ZnO films prepared by pyrosol process, however, our E_u values are higher. This may be due to the difference in the method of preparation as well as the preparation conditions.

3.4. Electrical properties

Fig. 11 shows the temperature (T) dependence of the electrical conductivity (σ) measured in temperature range 300–600 K for the undoped and In-doped ZnO nanostructures.

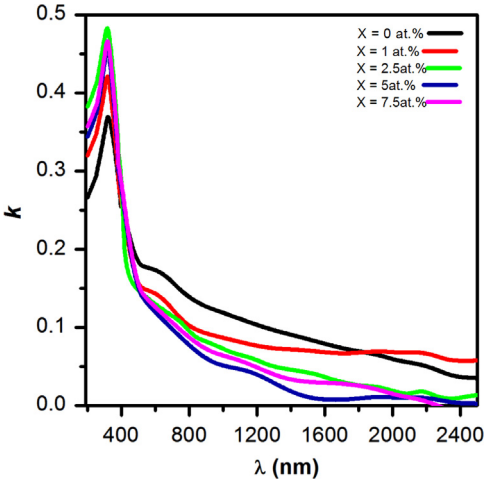

Fig. 9. Extinction coefficient variations with wavelength for the undoped and In- doped ZnO nanostructures.

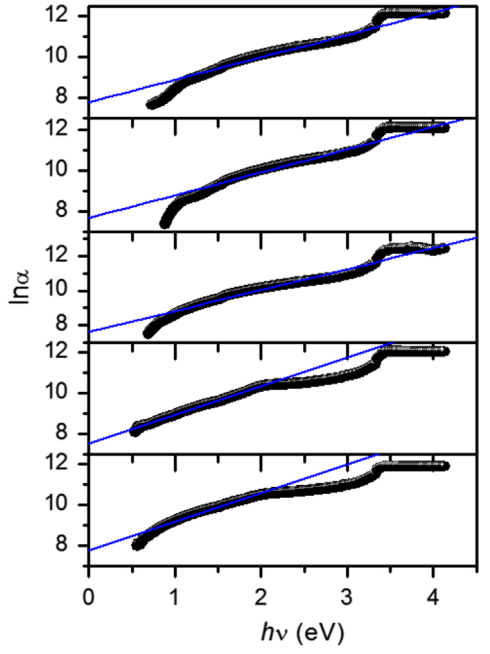

Fig. 10. lnα as a function of photon energy for the undoped and In-doped ZnO nanostructures.

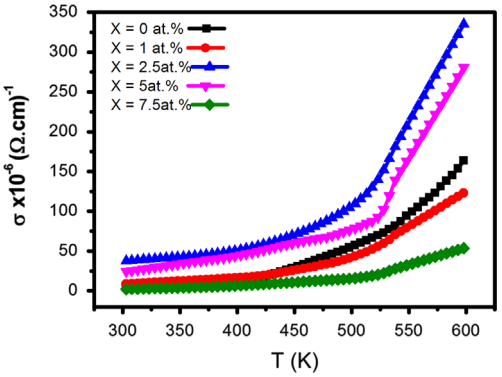

Fig. 11. The temperature dependence of the electrical conductivity for undoped and In-doped ZnO nanostructures.

The results demonstrate the semiconducting behavior of all the materials under study where by increasing the temperature, more and more charge carriers can overcome the energy barrier and participate in the electrical conduction [25]. To show the influence of In doping on the electrical conductivity of ZnO, the room temperature electrical conductivity σ_{300} was plotted as a function of the In content in Fig. 12. As known, effective doping is achieved when ionic radius of the dopant is the same as or smaller than that of the host ion [26]. The ionic radius of Zn^{+2} and In^{+3} are approximately the same which enables indium ions to be incorporated in interstitial and takes substitution positions introducing more and more effect carriers as the indium increases. This explains the enhancement of the σ_{300} values as In content increases to $x=2.5$ at%. With further In doping ($x=5$ and 7.5 at%), although the donors action is in increasing, the solubility limits of indium in ZnO leads to segregation of the dopant in the form of In_2O_3 phase, which acts as trapping for the free carriers leading to the decrease of conductivity. It is worth mentioning that the conductivity values of our composition are (10^{-4}–$10^{-5}\,\Omega^{-1}\,cm^{-1}$) lower than values reported elsewhere [26,27]. This inconsistency may be ascribed to the following factors:

1- Our compositions are nearly stoichiometric, which means they include less oxygen vacancies. Stoichiometry deviation originated from oxygen deficiency increases the charge carrier density [28].
2- The conductivity values are greatly influenced by the thickness of the film. The thickness of our films was ~400 nm. Low thickness films mean low electrical conductivity values.
3- Deposition techniques, annealing temperature and annealing environment like vacuum annealing, nitrogen, hydrogen, oxygen, air, etc, are also factors affect the conductivity values [27]. Our films have been subjected to high temperature annealing during preparation.

The σ–T plots were found to be well represented by Arrhenius equation:

$$\sigma = \sigma_0 \exp\left(-E_a/K_BT\right) \quad (5)$$

where σ_0 is the pre-exponential factor including the charge carrier mobility and density of state, E_a is the activation energy for electrical conduction, which is a function of the electronic energy levels of the chemically interacting atoms in the materials and K_B is the Boltzmann's constant. The linear behavior of lnσ versus 1000/T plots (Fig. 13) confirms the well-fitting of the σ–T data with Eq. (5). However, each lnσ versus 1000/T plot consists of two straight lines with different slopes suggesting a transition between two different conduction mechanisms. This transition appears at certain temperature T_σ which was found to be dependent on the In content in the compositions. The activation energies E_{ah} and E_{al} corresponding to the high temperature and low temperature ranges, respectively, were determined and plotted as functions in the In content in Fig. 14. Note that, values of E_{ah} and E_{al} agree well with previous reported results [29,30]. The E_{ah} values increase with increasing the In content and then decrease, where the x=5 at% sample possesses the highest activation energy in coincidence with the data recorded for the optical energy gap E_g. Nevertheless, the activation energy E_{al} corresponds to the low temperature range behaves in different manner where it decreases as the In content increases from x=0 to 2.5 at%. With higher indium content (x=5 and 7.5 at%) although free carriers is in increasing, phase separation of indium oxide acts as trapping for the free carriers (as revealed by XRD analysis), that rises the activation energy values.

The activation energy corresponds to the low temperature range is associated with one of two possible donor ionization processes. The first is In ions substitution that act as shallow donors near the conduction band [31]. The second is zinc interstials (Zn_i) ionization ($Zn_i^+ \rightarrow Zn_i^{++} + e^-$) proposed by Sukker and Tuller [32]. Although Zn_i were subsequently considered as intermediate donor levels in the band gap, the low migration barrier required for their diffusion is 0.57 eV, that are responsible for the fast recovery of the electrical properties [33]. The high temperature activation energy can be associated with oxygen vacancies ($V_o \rightarrow V_o^+ + e^-$) as proposed by Simpson and Cordaro [34]. The second is the desorption of O_2^- species according to the equation $O_2^- \rightarrow O_2 + e^-$ [2]. Existence of the activation energies at low and high temperature regions suggests the presence of two donor levels. These levels are shallow (correspond to E_{al}) and deep (correspond to E_{ah}) donor levels in the band gap of the ZnO semiconductor. Thus in the high temperature region, the electrical conduction of the ZnO is thermally activated from the deep level to the conduction band while in the low temperature region it is activated from the shallow level. This explains the low values of E_{al} compared to E_{ah} [35].

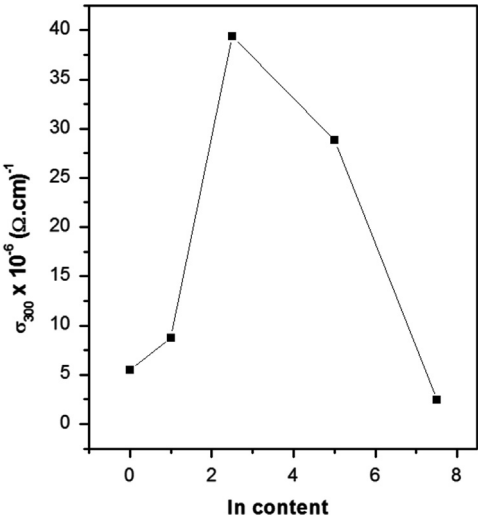

Fig. 12. Variation of room temperature conductivity σ_{300} with In content.

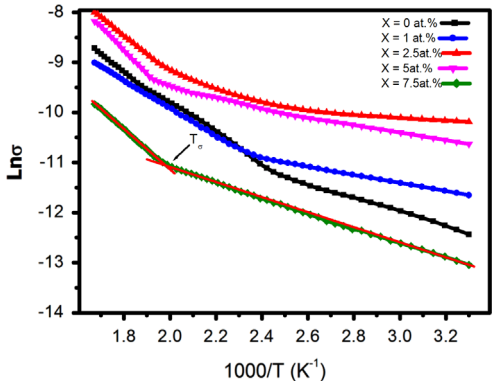

Fig. 13. variation of ln σ with temperature for undoped and In-doped ZnO nanostructures.

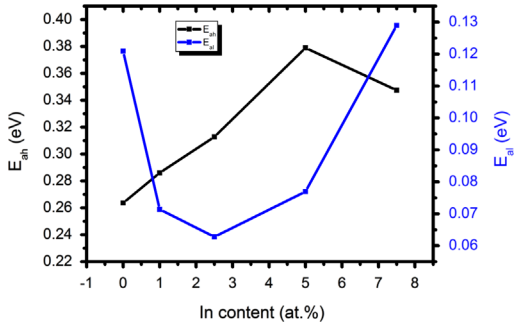

Fig. 14. Activation Energies variation at high (E_{ah}) and low (E_{al}) temperature ranges.

To prove the domination of the thermal activation conduction in our samples, the pre-exponential factor was determined. The pre-exponential factor detects whether the conduction is extended or by hoping. As was suggested by Davis and Mott [36], the pre-exponential factor for conduction in localized state should be two or three orders smaller in magnitude than for conduction in extended states and should become smaller for conduction in localized states near the Fermi level. If the value of the pre exponential factor is in the range 10^3–$10^4\ \Omega^{-1}\,cm^{-1}$, the conduction is mostly in extended states. A smaller value of pre-exponential factor would indicate a wide range of localized states and conduction by hoping. In our samples, values of σ_0 for undoped and doped samples vary from 2.2×10^3 to $7.26 \times 10^3\ \Omega^{-1}\,cm^{-1}$. This suggests that the conduction is due to thermally assisted charge carrier movement in the extended states.

4. Conclusion

Well crystallized undoped and In doped ZnO nanostructures were prepared by vapor transport method. The addition of In has a significant impact on the gradual transformation of nanowires to nanoflower. This is caused by the redistribution of surface energy which changes the crystal growth direction. X-ray and Raman spectroscopy demonstrated that indium addition doesn't change the wurtzite structure of ZnO nanostructures. The Burstein–Moss effect were observed for indium values from $x=1$ up to $x=5$ at% while the higher indium content ($x=7.5$ at%.) causes band shrinkage. Values of extinction coefficient and refractive index are also affected strongly by In addition. The activation energy values change according to the indium content as well as the temperature range taken in consideration.

Acknowledgment

The authors are grateful to Prof. B. Büchner and Dr. A. Leonhardt, Leibniz Institute for Solid State and Materials Research (IFW), Dresden, Germany for providing Raman spectroscopy analyses.

References

[1] A.E. Morales, M.H. Zaldivar, U. Pal., Indium doping in nanostructured ZnO through low-temperature hydrothermal process, Opt. Mater. 29 (2006) 100–104.
[2] J. Shi, X. Wang, Functional semiconductor nanowires via vapor deposition, J. Vac. Sci. Technol. B 29 (2011) 060801–060821.
[3] M. Ahmad, J. Zhao, J. Iqbal, W. Miao, L. Xie, R. Mo, J. Zhu, Conductivity enhancement by slight indium doping in ZnO nanowires for optoelectronic applications, J. Phys. D: Appl. Phys. 42 (2009) 165406–165407.
[4] S.Y. Lim, S. Brahma, C.-P. Liu, R.-C. Wang, J.-L. Huang, Effect of indium concentration on luminescence and electrical properties of indium doped ZnO nanowires, Thin Solid Films 549 (2013) 165–171.
[5] M. Rezapour, N. Talebian, Synthesis and investigation of Indium doping and surfactant on the morphological, optical and UV/Vis photocatalytic properties of ZnO nanostructure, Ceram. Int. 40 (2014) 3453–3460.
[6] Y. Imanishi, M. Taguchi, K. Onisaw, Effect of sublayer surface treatments on ZnO transparent conductive oxides using dc magnetron sputtering, Thin Solid Films 518 (2010) 2945–2948.
[7] F. Cai, L. Zhu, H. He, J. Li, Y. Yang, X. Chen, Z. Ye, Growth and optical properties of tetrapod-like indium-doped ZnO nanorods with a layer-structured surface, J. Alloys Compd. 509 (2011) 316–320.
[8] S.T. Lee, T.I. Jeon, H. Makino, J.H. Chang, Field emission properties of indium-doped ZnO tetrapods, Curr. Appl. Phys. 9 (2009) e169–e172.
[9] S.S. Shinde, P.S. Shinde, C.H. Bhosale, K.Y. Rajpure, Optoelectronic properties of sprayed transparent and conducting indium doped zinc oxide thin films, J. Phys. D: Appl. Phys. 41 (2008) 105109, P6.
[10] S.S. Badadhe, I.S. Mulla, H_2S gas sensitive indium-doped ZnO thin films: preparation and characterization, Sens. Actuators, B 143 (2009) 164–170.
[11] G. Singh, S.B. Shrivasava, D.I. Jain, S. Pandya, T. Shripathi, V. Ganesan, Effect of indium doping on zinc oxide films prepared by chemical spray pyrolysis technique, Bull. Mater. Sci. 33 (2010) 581–587.
[12] Y.Q. Chang, P.W. Wang, S.L. Ni, Y. Long, X.D. Li, Influence of Co content on Raman and photoluminescence spectra of Co doped ZnO nanowires, J. Mater. Sci. Technol. 28 (2012) 313–316.
[13] W.-H. Zhang, W.-D. Zhang, Synthesis and optical properties of nanosheet-based rh-In_2O_3 microflowers by triethylene glycol-mediated solvothermal process, J. Phys. Chem. Solids 74 (2013) 1271–1274.
[14] P.P. Palni, S. Kumari, N.G. Baruah, D.K. Singh, P.K. Giri, Effect of Annealing on high quality zinc oxide nanowires synthesized by catalytic vapor-deposition,, Nano Trends: J. Nanotechnol. Appl. 3 (2007) 1–6.
[15] R. Yousefi, F. Jamali-Sheini, A.K. Zakc, M.R. Mahmoudi, Effect of indium concentration on morphology and optical properties of In-doped ZnO nanostructures, Ceram. Int. 38 (2012) 6295–6301.
[16] W. Li, E. Shi, W. Zhong, Z. Yin, Growth mechanism and growth habit of oxide crystals, J. Cryst. Growth 203 (1999) 186–196.
[17] M. Fox, Optical Properties of Solids, Oxford University Press, 2001, p. 10.
[18] J.C. Tauc, Optical Properties of Solids, North-Holland, Amsterdam, 1972.
[19] L. Nevot, P. Croce, Caractérisation des surfaces par réflexion rasante de rayons X. Application à l'étude du polissage de quelques verres silicates, Rev. Phys. Aplique 15 (1980) 761–779.
[20] L.M. Li, C.C. Li, J. Zhang, Z.F. Du, B.S. Zou, H.C. Yu, Y.G. Wang, T.H. Wang, Band gap narrowing and ethanol sensing properties of In-doped ZnO nanowires, Nanotechnology 18 (2007) 225504–225508.
[21] X.C. Wang, X.M. Chen, B.H. Yang, Microstructure and optical properties of polycrystalline ZnO films sputtered under different oxygen flow rates, J. Alloys Compd. 488 (2009) 232–237.
[22] G.P. Palmer, K.R. Poepplmeier, T.O. Mason, Conductivity and transparency of ZnO/SnO_2-cosubstituted In_2O_3, Chem. Mater. 9 (1997) 3121–3126.
[23] M.S. Tokumoto, A. Smith, C.V. Santilli, S.H. Pulcinelli, A.F. Craievich, E. Elkaim, A. Traverse, V. Briois, Structural electrical and optical properties of undoped and indium doped ZnO thin films prepared by the pyrosol process at different temperatures, Thin Solid Films 416 (2002) 284–293.
[24] V. Srikant, D.R. Clarke, Optical absorption edge of ZnO thin films: the effect of substrate, J. Appl. Phys. 81 (1997) 6357–6364.
[25] S. Ilican, Y. Caglar, M. Caglar, F. Yakuphanoglu, Electrical conductivity, optical and structural properties of indium-doped ZnO nanofiber thin film deposited by spray pyrolysis method, Physica E 35 (2006) 131–138.
[26] B. Joseph, P.K. Manoj, V.K. Vaidyan, Studies on preparation and characterization of indium doped zinc oxide films, Bull. Mater. Sci. 28 (2005) 487–493.
[27] V. Shelke, M.P. Bhole, D.S. Patil, Opto-electrical characterization of transparent conducting sand dune shaped indium doped ZnO nanostructures, J. Alloys Compd. 560 (2013) 147–150.
[28] N. Al Dahoudi, A. AlKahlout, S. Heusing, P. Herbeck-Engel, R. Karos, P. Oliveira, Indium doped zinc oxide nanopowders for transparent conducting coatings on glass substrates., J. Sol-Gel Sci. Technol. 67 (2013) 556–564.
[29] C.S. Naveen, M.L. Dinesha, H.S. Jayanna, Effect of fuel to oxidant molar ratio on structural and DC electrical conductivity of ZnO nanoparticles prepared by simple solution combustion method, J. Mater. Sci. Technol. 29 (2013) 898–902.
[30] S.L. Patil, M.A. Chougule, S.G. Pawar, B.T. Raut, S. Sen, V.B. Patil, New process for synthesis of ZnO thin films: microstructural, optical and electrical characterization, J. Alloys Compd. 509 (2011) 10055–10061.
[31] H. Duan, H. He, L. Sun, S. Song, Z. Ye, Indium-doped ZnO nanowires with infrequent growth orientation, rough surfaces and low-density surface traps, Nanoscale Res. Lett. 8 (2013) 493–496.
[32] M.H. Sukker, H.L. Tuller, Defect equilibria in ZnO varistor materials, Adv. Ceram. 7 (1984) 49–55.
[33] A. Janotti, C.G. Van de Walle, Fundamentals of zinc oxide as a semiconductor, Rep. Prog. Phys. 72 (2009) 126501–126529.
[34] J.C. Simpson, J.F. Cordero, Characterization of deep levels in zinc oxide, J. Appl. Phys. 63 (1988) 1781–1783.
[35] M. Caglar, S. Ilican, Y. Caglar, F. Yakuphanoglu, Electrical conductivity and optical properties of ZnO nanostructured thin film, Appl. Surf. Sci. 255 (2009) 4491–4496.
[36] N.F. Mott, E.A. Davis, Electronics Processes in Non-Crystalline Materials, Clarendon, Oxford, 1979.